

TWO VIEWS OF THE SAME PROBLEM: AEROSERVOELASTICITY FROM A CONTROLS AND FLUTTER PERSPECTIVE

Raj K. Narisetti¹, Paul F. Taylor², and Jerry Newsom³

¹ Gulfstream Aerospace Corp.,
Savannah, Georgia, 31402, USA
rajkumar.narisetti@gulfstream.com

² Gulfstream Aerospace Corp.,
Savannah, Georgia, 31402, USA
paul.taylor@gulfstream.com

³ Newsom Aerospace Consulting LLC
Poquoson, Virginia, 23662, USA
jnewsom123@gmail.com

Keywords: closed loop flutter, aeroservoelasticity, broken loop analysis.

Abstract: The current paper examines the aeroservoelastic stability problem from both the perspective of the Flight Controls Engineer and the Flutter Engineer and shows that both are solving the same problem. The advantages and disadvantages of each strategy are described along with recommendations for usage in an aircraft design environment.

1 INTRODUCTION

Aeroservoelastic (ASE) analysis builds upon the interaction of flexible aircraft and unsteady aerodynamic forces (aeroelastic analyses), by adding the influence from the aircraft flight control system. As aircraft become more flexible and flight controls operate at higher bandwidths, the possibility of adverse feedback, leading to instability becomes more likely and requires ASE stability analyses during the design phase.

Aeroelastic systems are typically modeled as systems of 2nd order differential equations. These systems provide representations of spatial distributions of mass, stiffness, damping and aerodynamic forces. Converting these systems into a state space form allows a conceptually straightforward method for determining system stability via extraction and examination of the so-called 'A' or system matrix eigenvalues. For system stability, all of the eigenvalues must lie in the left half of the complex plane. The behavior of the aeroelastic system can be augmented and modified by including the effects of feedback controllers. This process simply extends the state space formulation to include the state space matrices of the controller. The stability assessment can then be extended to include the effects of the controller(s). Various analytical, numerical and test procedures exist to predict the aeroservoelastic stability of aircraft [1–4].

In the following, two different approaches will be discussed to establish the stability of an aeroservoelastic system. Broken loop frequency response analysis and closed loop flutter analysis are two primary techniques one can utilize to assess the ASE stability of the system.

This paper also shows the mathematical equivalence between broken loop frequency response analysis and the closed loop flutter analysis.

Traditional flutter analysis typically involves iterative eigenvalue procedures such as PK-method, K-method, KE-method and the G-method which have been widely utilized in the industry to solve the classic aeroelastic equations of motion. The iterative nature of the eigenvalue formulation is due to unsteady aerodynamic forces being represented as tables of complex values as a function of reduced frequency. Such methods generate complex eigenvalues and the aeroelastic stability is analyzed using dynamic pressure dependent modal frequency and damping curves (VGF plots). To analyze the ASE stability via closed loop flutter analysis, the controller dynamics (control law) are typically represented in state-space matrix form or cascaded second order systems and the iterative methods (such as PK-method) can be extended to include the controller dynamics into the aeroelastic equations of motion. In addition to flexible modes, the control law degrees of freedom are introduced into the aeroelastic equations making the problem even more complicated to track and identify the resulting complex eigenvalues.

The frequency domain analysis approach is more of control-centric view of the ASE stability problem. This approach utilizes broken loop frequency domain analysis to determine closed loop stability based on the open loop transfer function [5]. The closed loop stability assessment is primarily based on the phase and gain margin study of the frequency response functions emanating from the aircraft aeroelastic response and the control law transfer functions. For a given flight point, this method directly shows the closed loop stability [2] and additionally indicates the robustness of the closed loop system by depicting the gain and phase margins. One of the primary advantages of this approach is that it allows the analyst to assess the ASE stability and robustness for all aeroelastic modes at the same time. This would be equivalent to a very large number of closed loop flutter runs. The method also provides an efficient way to assess the various control law configurations by merely interchanging the controller frequency response functions (FRFs).

This paper describes the two approaches used in predicting aeroservoelastic stability:

1. Closed loop PK flutter analysis – flutter perspective
2. Broken loop frequency response analysis – controls perspective

The paper then presents several examples to illustrate the equivalence between the two methods. The first example considers a simple cantilevered plate model with a trailing edge control surface. The second example considers a more complex model representing a generic business jet (although for simplicity only a half-model is considered). In both cases, a simple control law is provided to modify the control surface deflection as a function of tip position or acceleration. This control law can be modified to examine the cause and effect. The paper demonstrates that the aeroservoelastic stability can be assessed using both methods.

Section 2 describes the two methods and their mathematical equivalence. Section 3, Section 4 and Section 5 detail the example aeroelastic models and their respective closed loop stability analyses. Each example shows aeroservoelastic stability using both methods with modifications to the respective control law. Section 6 presents the concluding remarks along with some details regarding merits and demerits of each approach. Note that the parameters of the sample problems presented in this paper are arbitrary and are intended to demonstrate the validity of the process.

2 AEROSERVOELASTIC STABILITY

This section presents the two techniques used in assessing the aeroservoelastic stability. An extension to the PK flutter analysis to include the controller dynamics is described first, followed by the broken loop frequency response analysis.

2.1 Closed Loop Flutter Analysis

A common technique which is widely used involves transforming the controller dynamics into a series of second order cascaded models which can then directly be integrated into the aeroelastic equations of motion [6]. The technique presented here shows a slightly different approach where the controller dynamics can be used directly in state space form without transforming into a system of cascaded second order transfer functions.

Consider the aeroelastic equations of motion in the Laplace domain [7],

$$\left[M_{hh}s^2 + \left(B_{hh} - \frac{1}{4}\rho\bar{c}V Q_{hh}^I/k \right) s + \left(K_{hh} - \frac{1}{2}\rho V^2 Q_{hh}^R \right) \right] \{q_h(s)\} = F_{h\delta}(s) \quad (1)$$

where M_{hh} , B_{hh} and K_{hh} are generalized mass, damping and stiffness matrices. $Q_{hh}(m, k) = Q_{hh}^R + iQ_{hh}^I$ represents the unsteady aerodynamic force matrix which is dependent on Mach number m and reduced frequency k . The vector q_h denotes the generalized degrees of freedom and $F_{h\delta}(s)$ represents the control mode coupling which can be expressed by the following equation:

$$F_{h\delta}(s) = \left(-\frac{1}{2}\rho V^2 Q_{h\delta}^R \right) q_c(s) + s \left(-\frac{1}{4}\rho\bar{c}V Q_{h\delta}^I/k \right) q_c(s) - s^2 M_{h\delta} q_c(s) \quad (2)$$

where $Q_{h\delta}(m, k) = Q_{h\delta}^R + iQ_{h\delta}^I$ denotes the control surface aerodynamic coupling, $M_{h\delta}$ represents the control surface inertial coupling. The underlying assumptions required in arriving at Equations 1 and 2 can be reviewed in [7].

Equations 1 and 2 can be recast into state space form in the following way,

$$\begin{aligned} \dot{x}_p &= A_p x_p + B_p u_p \\ y_p &= C_p x_p + D_p u_p \end{aligned} \quad (3)$$

where the state space matrices A_p and B_p can be given by,

$$A_p = \begin{bmatrix} 0 & I \\ -M_{hh}^{-1} \left(K_{hh} - \frac{1}{2}\rho V^2 Q_{hh}^R \right) & -M_{hh}^{-1} \left(B_{hh} - \frac{1}{4}\rho\bar{c}V Q_{hh}^I/k \right) \end{bmatrix} \quad (4)$$

$$B_p = \begin{bmatrix} 0 & 0 & 0 \\ M_{hh}^{-1} \left(\frac{1}{2}\rho V^2 Q_{h\delta}^R \right) & M_{hh}^{-1} \left(\frac{1}{4}\rho\bar{c}V Q_{h\delta}^I/k \right) & -M_{hh}^{-1} M_{h\delta} \end{bmatrix} \quad (5)$$

and the state vector x_p consists of displacements and velocities of generalized degrees of freedom $[q_h^{disp} \ q_h^{vel}]^T$. A typical sensor response y_p can be formulated as the following,

$$y_p = \begin{bmatrix} \text{position} \\ \text{velocity} \\ \text{acceleration} \end{bmatrix} \quad (6)$$

y_p can be either a translation or angular quantity. Corresponding to the above definition of the sensor output, matrices C_p and D_p take the following form,

$$C_p = \begin{bmatrix} \Phi_{sensor}^T & 0 \\ 0 & \Phi_{sensor}^T \\ [0 \ \Phi_{sensor}^T]A_p \end{bmatrix} \quad (7)$$

$$D_p = \begin{bmatrix} 0 & 0 \\ 0 & 0 \\ [0 \ \Phi_{sensor}^T]B_p \end{bmatrix} \quad (8)$$

Next, the controller dynamics including the actuator dynamics can be represented by the following equations. The input to the control law is the sensor response y_p and the output typically denotes the control surface position,

$$\begin{aligned} \dot{x}_c &= A_c x_c + B_c u_c \\ y_c &= C_c x_c + D_c u_c \end{aligned} \quad (9)$$

With the control law in the feedback loop, the inputs $u_c = y_p$ and $u_p = y_c$ and the closed loop state matrix can be given by the following equation:

$$\begin{Bmatrix} \dot{x}_p \\ \dot{x}_c \end{Bmatrix} = \begin{bmatrix} A_p + B_p F^{-1} D_c C_p & B_p F^{-1} C_c \\ B_c C_p + B_c D_p F^{-1} D_c C_p & A_c + B_c D_p F^{-1} C_c \end{bmatrix} \begin{Bmatrix} x_p \\ x_c \end{Bmatrix} \quad (10)$$

where, $F = I - D_c D_p$. Next, for a specific flight condition, the algorithm proceeds to compute the eigenvalues of the closed loop state matrix iteratively on the reduced frequency k and the solution is reached when the k value is within a very small tolerance to one of the eigenvalues. Note that the system order is now increased by the size of the controller plant matrix A_c .

Another common approach to solving the closed loop flutter problem is to use rational functional approximation for the unsteady aerodynamics [8–12]. Methods such as Roger's approximation [10], Matrix Pade approximation [11] or Karpel's minimum state method [12] can be implemented to transform the discrete k dependent aerodynamic force into a continuous one. This approximation can then be transformed back into the time domain where the unsteady aerodynamics is represented by the lag states. Irrespective of the technique, the aeroelastic equations can be expressed in the form shown by Equation 3 although the matrices A_p and B_p are formulated differently as compared to Equations 4 and 5. Note that the state matrix A_p is not dependent on the reduced frequency k . In this case, the state vector

x_p consists of displacements and velocities of generalized degrees of freedom as well as the aerodynamic lag states $[q_h^{disp} \ q_h^{vel} \ q_a]^T$. The stability of the closed loop system can be predicted by directly solving the eigenvalues of the closed loop state matrix (as given by Equation 9) without any iterative process.

2.2 Broken Loop Frequency Response Analysis

This approach is more of a controls centric view of examining the aeroservoelastic stability. In control engineering, the stability margins of a feedback closed loop system can be predicted by the open loop system frequency response function (FRF). Gain and phase margin analysis is ubiquitous in controls engineering and the stability margins indicate the response characteristics robustness of the stability of the closed loop system. Consider the linear aeroelastic plant dynamics governed by Equation 3. The open loop transfer function $G_p(s)$ can be written as,

$$G_p(s) = C_p(sI - A_p)^{-1}B_p + D_p \quad (11)$$

The control law transfer function can also be expressed similar to Equation (9) in the following form,

$$G_c(s) = C_c(sI - A_c)^{-1}B_c + D_c \quad (12)$$

For clarity, $G_p(s)$ refers to an open loop system throughout the document. Consider a generic single loop aeroservoelastic system, where $G_p(s)$ denotes the plant dynamics, $G_c(s)$ represents the controller dynamics and a simple gain feedback as shown in Figure 1,

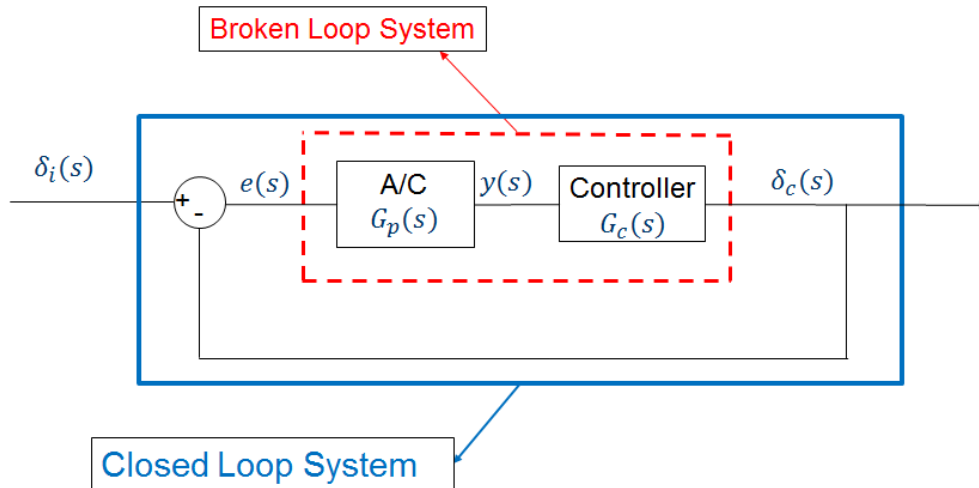


Figure 1: Generic closed loop aeroelastic system

In the above figure, δ_i denotes the control surface input, $y_p(s)$ denotes sensor output and δ_c denotes the control surface output. For a specific altitude and Mach number, the open loop plant response $G_p(s)$ and the control law frequency response $G_c(s)$ are known quantities. The closed loop system transfer function from the control input to the control output can be written as,

$$\frac{\delta_c(s)}{\delta_i(s)} = \frac{G_c(s)G_p(s)}{1 + G_c(s)G_p(s)} \quad (13)$$

To assess the closed loop system stability, a broken loop system is considered as indicated by the red dashed lines in Figure 1. The broken loop transfer function can be written as,

$$\frac{\delta_c(s)}{e(s)} = G_c(s)G_p(s) \quad (14)$$

The closed loop system stability is determined by the poles of the closed loop transfer function indicated by Equation 13 and checking if any pole exists on the right half of the complex plane. Equivalently, the closed loop stability can be assessed with the phase and gain margins of a broken loop transfer function indicated by Equation 14. Gain and phase margins reveal the magnitude of additional gain or phase that can be allowed in the feedback before the closed loop system becomes unstable [5].

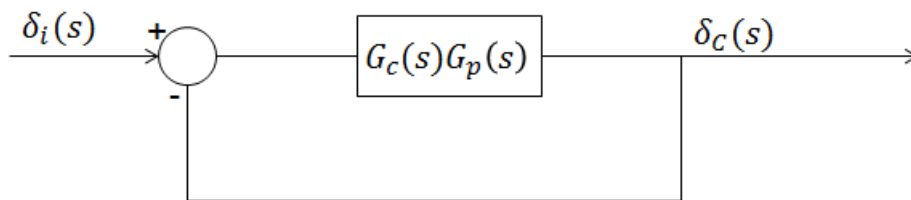


Figure 2: Broken loop system with unit gain feedback

3 SIMPLE TWO DOF PLATE MODEL

3.1 Model Description

The example problem consists of a simple rectangular unswept wing [13, 14]. The wing is rigid, but has two rotational springs at the root to provide flapping (θ) and pitch (α) degrees of freedom (see Figure 3). Model details can be found in the references.

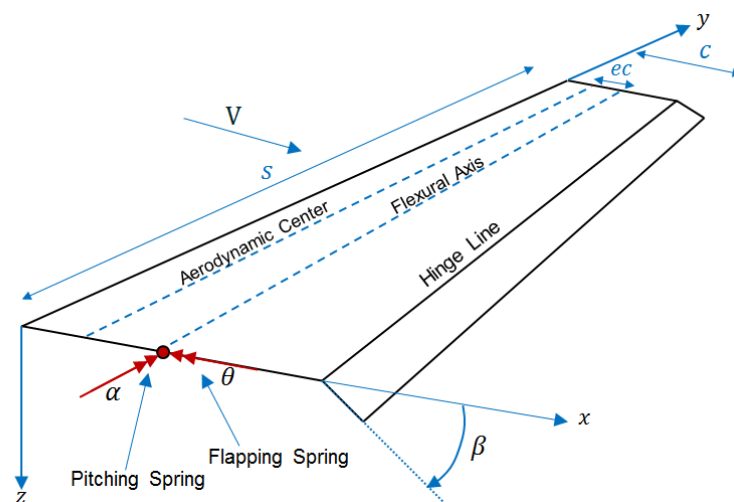


Figure 3: Simple two degree of freedom system

This two degree of freedom system uses quasi-steady aerodynamics, which is deemed sufficient for the illustrative purposes of this problem. The equations of motion can be shown to be:

$$M\ddot{q} + \rho V B_A \dot{q} + (\rho V^2 K_A + K_S)q = \rho V^2 K_C \beta \quad (15)$$

where, $q = [\theta \ \alpha]^T$, M is the inertia matrix, B_A is the aerodynamic damping matrix, K_A defines the aerodynamic stiffness matrix, K_S is the structural stiffness matrix and K_C represents the control surface aerodynamic stiffness matrix.

$$M = \begin{bmatrix} I_\theta & I_{\theta\alpha} \\ I_{\theta\alpha} & I_\alpha \end{bmatrix} \quad (16)$$

$$B_A = \begin{bmatrix} \frac{cs^3 a_w}{6} & 0 \\ \frac{-ec^2 s^2 a_w}{4} & \frac{-c^3 s}{8} M_{\dot{\alpha}} \end{bmatrix} \quad (17)$$

$$K_A = \begin{bmatrix} 0 & \frac{cs^2 a_w}{4} \\ 0 & \frac{-ec^2 s a_w}{2} \end{bmatrix} \quad (18)$$

$$K_S = \begin{bmatrix} K_\theta & 0 \\ 0 & K_\alpha \end{bmatrix} = \begin{bmatrix} (2\pi f_\theta)^2 I_\theta & 0 \\ 0 & (2\pi f_\alpha)^2 I_\alpha \end{bmatrix} \quad (19)$$

$$K_C = \begin{bmatrix} -cs^2 a_c & c^2 s b_c \end{bmatrix}^T \quad (20)$$

The wing chord is denoted by c , the wing span by s , a_w defines the wing lift curve slope, e represents non-dimensional eccentricity between aerodynamic and flexural axes, $M_{\dot{\alpha}}$ denotes the aerodynamic pitch damping term, a_c defines the control surface lift curve slope and b_c denotes the control surface pitching moment curve slope. An aerodynamic control surface is also provided to enable feedback and control the system dynamics. There is no inertial feedback associated with this control surface. The parameters for this study are provided in the following table:

Table 1: Simple Two DOF Model Parameters

Semi-span, s	7.5 m	Pitch damping coefficient, $M_{\dot{\alpha}}$	-1.2
Chord, c	2.0 m	Air density	1.225 kg/m ³
Flexural axis location	0.48c	Mass / unit area	100 kg/ m ²
Mass axis location	0.50c	Wing lift curve slope	6.2832/rad
Uncoupled flapping frequency	5.0 Hz	CS lift slope, a_c	2.487
Uncoupled torsion frequency	10.0 Hz	CS moment slope, b_c	-0.540

A simple control law is implemented, which utilizes displacement feedback of the flapping and pitch degrees of freedom to command the control surface deflection as follows:

$$\beta = K_d[s_0 - c/2]q \tag{21}$$

The open loop flutter speed is 154.35 m/s as seen in Figure 4.

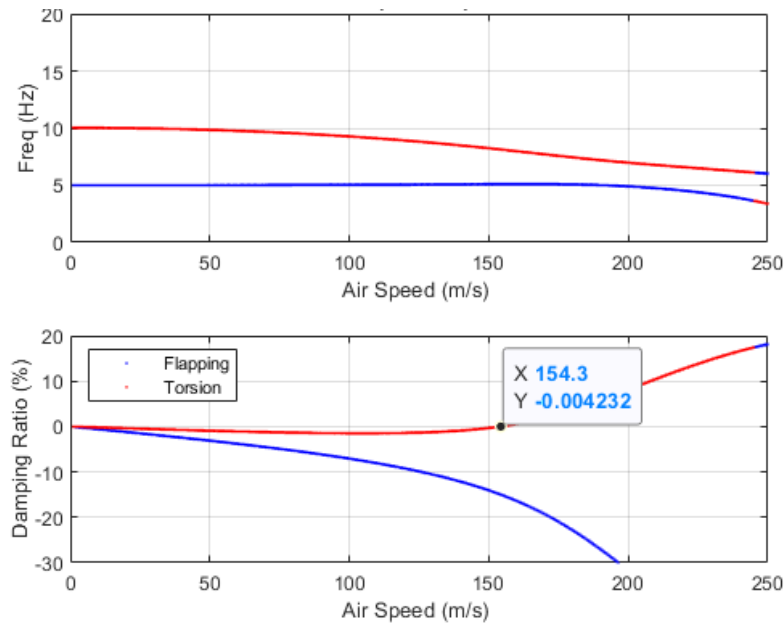


Figure 4: Open loop flutter solution

The closed loop system is implemented and broken loop analysis is accomplished by breaking the loop to the control surface input. At 100 m/s, the broken loop analysis shows that the closed loop system is stable and indicates the stability margin of ~11.1 dB. Figure 5 shows the root locus plot while the same information is displayed in a Bode plot (Figure 6).

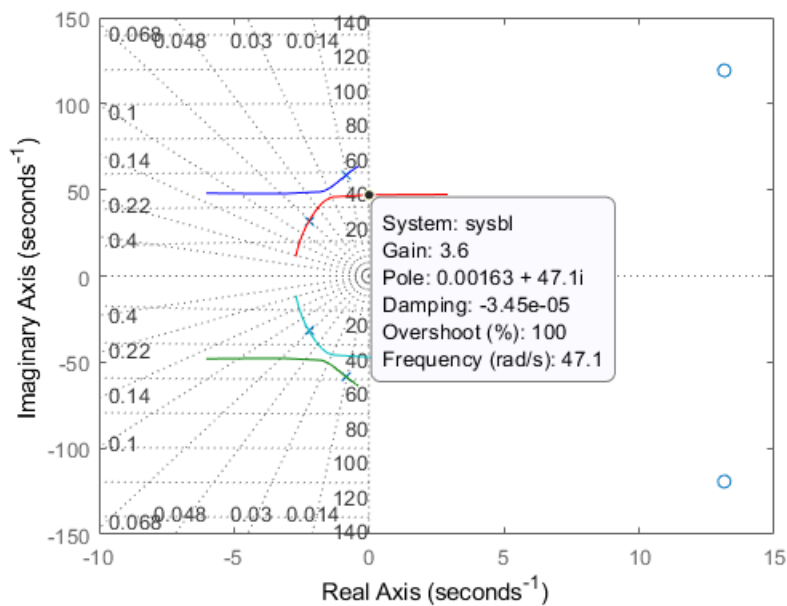


Figure 5: Broken loop root locus plot

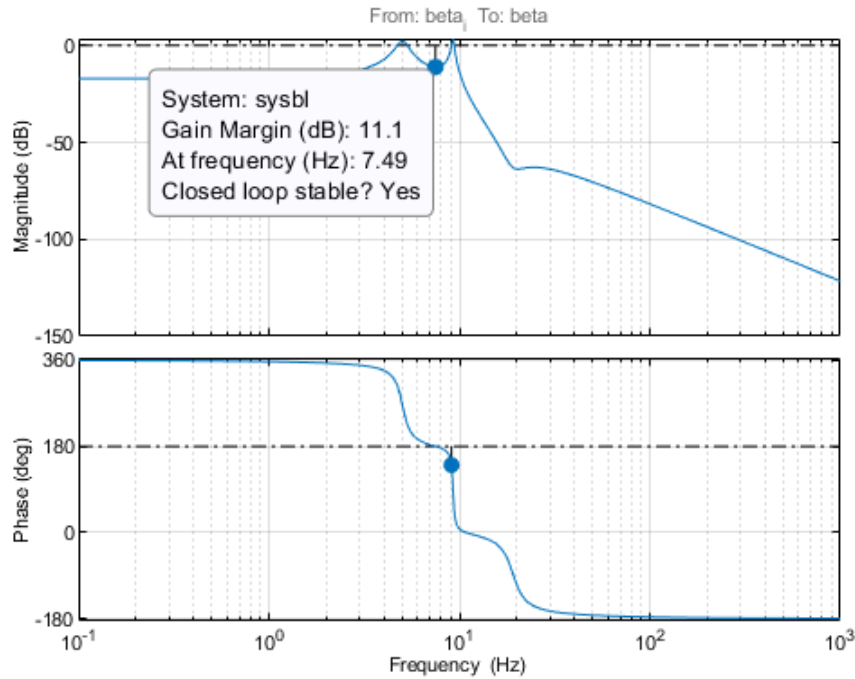


Figure 6: Broken loop frequency response analysis – Bode diagram

The stability margin computed via the broken loop analysis shows that the closed loop aeroelastic system is stable up to 11.1 dB at this flight condition (100 m/s). The stability check can be performed by changing the feedback gain value to 11.1 dB (or $K = 3.6$) and then performing a closed loop flutter analysis which results in the flutter velocity being 100 m/s (Figure 7) as predicted by the broken loop FRF approach.

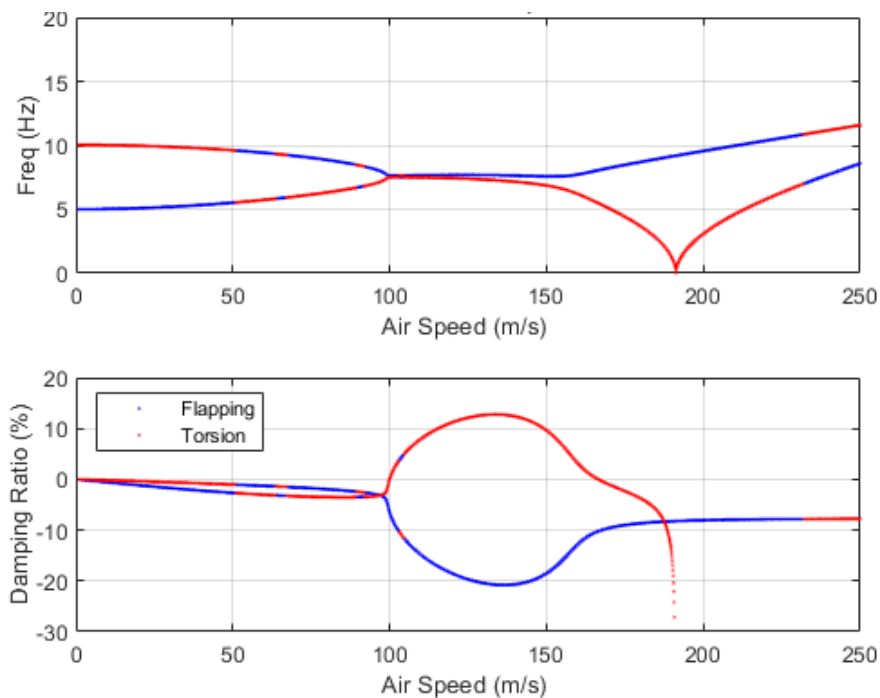


Figure 7: Closed loop flutter analysis with gain = 3.6

4 CANTILEVERD PLATE MODEL

4.1 Model Description

The example consists of a flat plate finite element model with a control surface attached to the trailing edge. The control surface rotational stiffness is modeled using CBUSH elements which can be modified to achieve a required frequency. The plate's main surface is cantilevered at the root modeled using the Nastran SPC entries. The two main primary modes of interest are the control surface rotation mode (~ 12 Hz) and the first bending mode with some control surface rotation (~ 56 Hz) shown in Figure 8 and Figure 9 respectively.

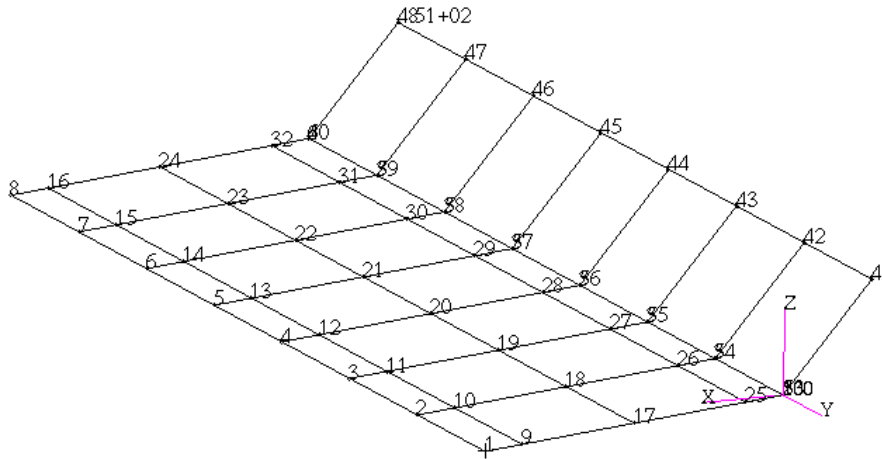


Figure 8: Control surface rotation mode ~ 9 Hz

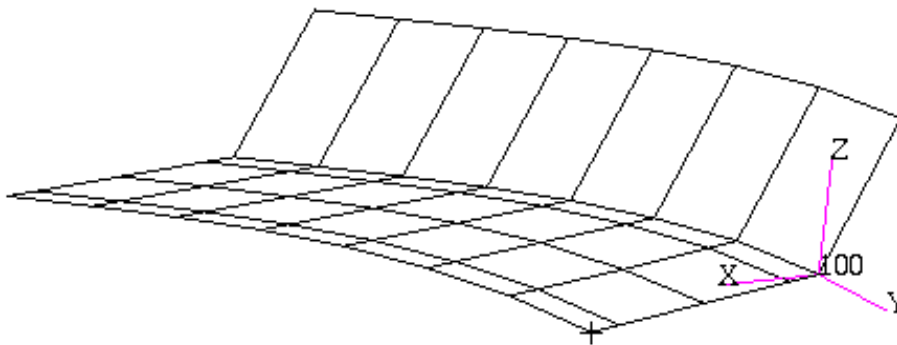


Figure 9: First bending mode with control surface rotation ~ 56 Hz

The unsteady aerodynamics is modeled using the doublet-lattice method. Uncontrolled (without a control system) flutter analysis at Mach 0.450 shows coupling of the two modes resulting in an unstable mode at approximately 56.8 keas. PK-method is employed to solve the aeroelastic equations and the resulting frequency-damping (VGF) curves are shown in Figure 10.

The frequency response functions are generated with the control surface position as the input and output being the positive z-displacement at the sensor grid 24 (wing tip). The subsequent sections present the stability analysis via 1) broken loop frequency response approach and 2) closed loop flutter analysis approach for three closed loop configurations. For all the configurations, sensor definition (24Z+) is unchanged.

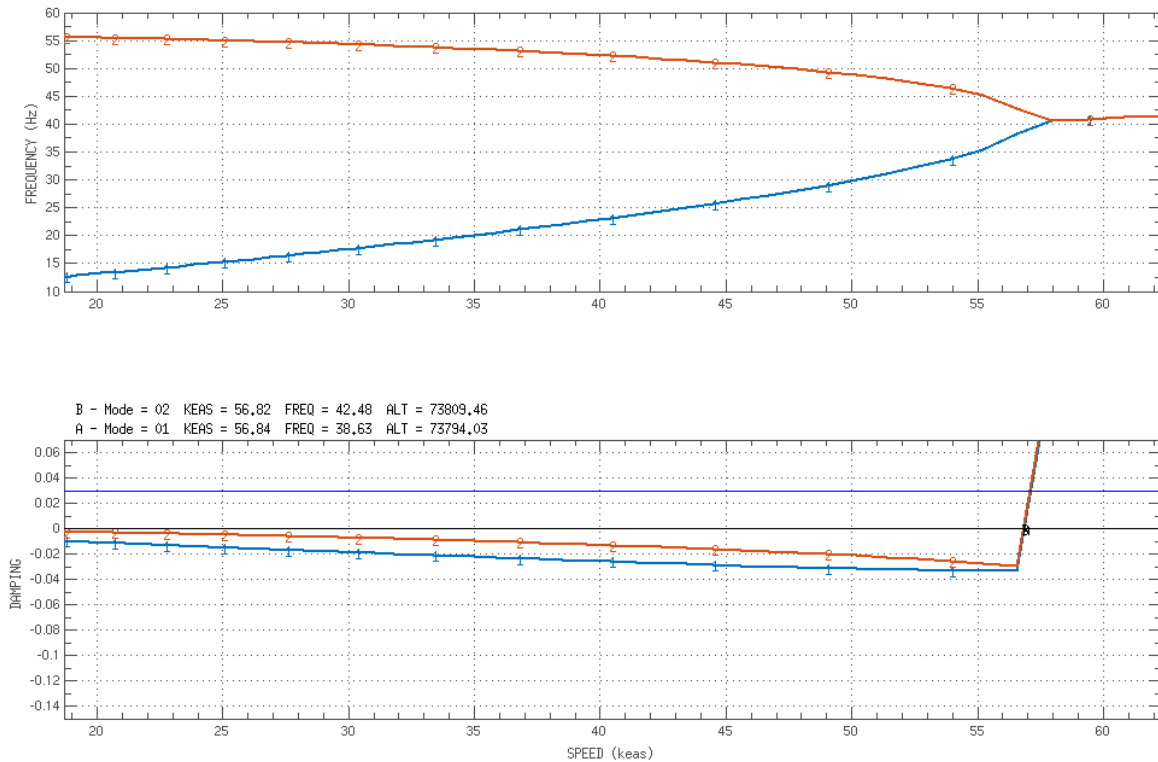


Figure 10: Open loop VGF plot at Mach 0.450

To generate the open loop frequency response, state-space formulation of the aeroelastic model was utilized which was derived using Roger's method. The number of lag roots was set to 8 and the inertial coupling was omitted from the analysis. To generate the aeroelastic frequency response functions, rational function approximation of the unsteady aerodynamics is not necessary but it is done so here in this work for convenience purposes.

For every configuration, the following steps are executed:

1. A control law is designed at the open loop flutter speed
2. The same control law is applied at a different flight condition or dynamic pressure
3. Broken loop frequency response from control input to control output is generated
4. Stability margins are computed
5. For gain margin, the control law is modified by multiplying the gain margin
6. For phase margin, approximate Pade filter is designed to introduce the delay
7. Closed loop PK flutter analysis is run with the modified control law
8. Instability is shown to occur at the flight condition selected in Step 2.

4.2 Configuration # 1

The control law transfer function from sensor position 24Z+ to control surface output is given by the following equation:

$$G_c(s) = \frac{0.01s^2 + 10s + 1}{s^2 + 2s + 1} \quad (22)$$

The details of this configuration are presented in the following table:

Table 2: Cantilevered Beam Example – Configuration 1

Broken Loop Frequency Response	Mach 0.450 at 51.4 keas GM = 5.07 dB at 31.2 Hz
Closed Loop Flutter Analysis	Mach 0.450 - PK Method Control Law Gain Scaled by 5.07 dB Flutter Speed ~ 51.8 keas at 31.4 Hz

Figure 11 shows the broken loop frequency response plot at 51.4 keas. The plot also indicates the gain margin ~ 5.07 dB in the closed loop system. The control law is modified by scaling the scaling the control law (Equation 22) by the resulting gain margin. This gain scaled control law is then implemented in the closed flutter analysis via the PK method (Figure 12).

The flutter crossing now occurs at 51.8 keas which is approximately 0.8% higher than the expected value (51.4 keas). This numerical difference occurs due to the way the broken loop frequency response is computed in comparison to the way the flutter analysis was performed. The open loop response is computed using state space formulation (Roger's rational function approximation) whereas the closed loop flutter was performed via the iterative PK method.

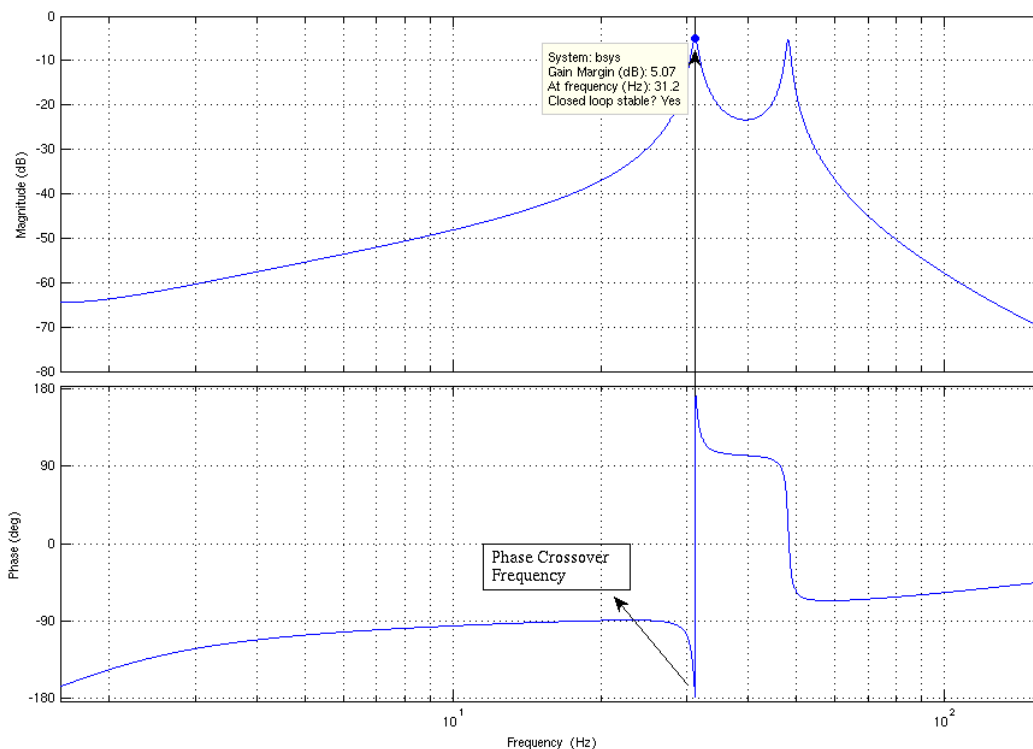


Figure 11: Broken loop stability at Mach 0.450 and 51.4 keas

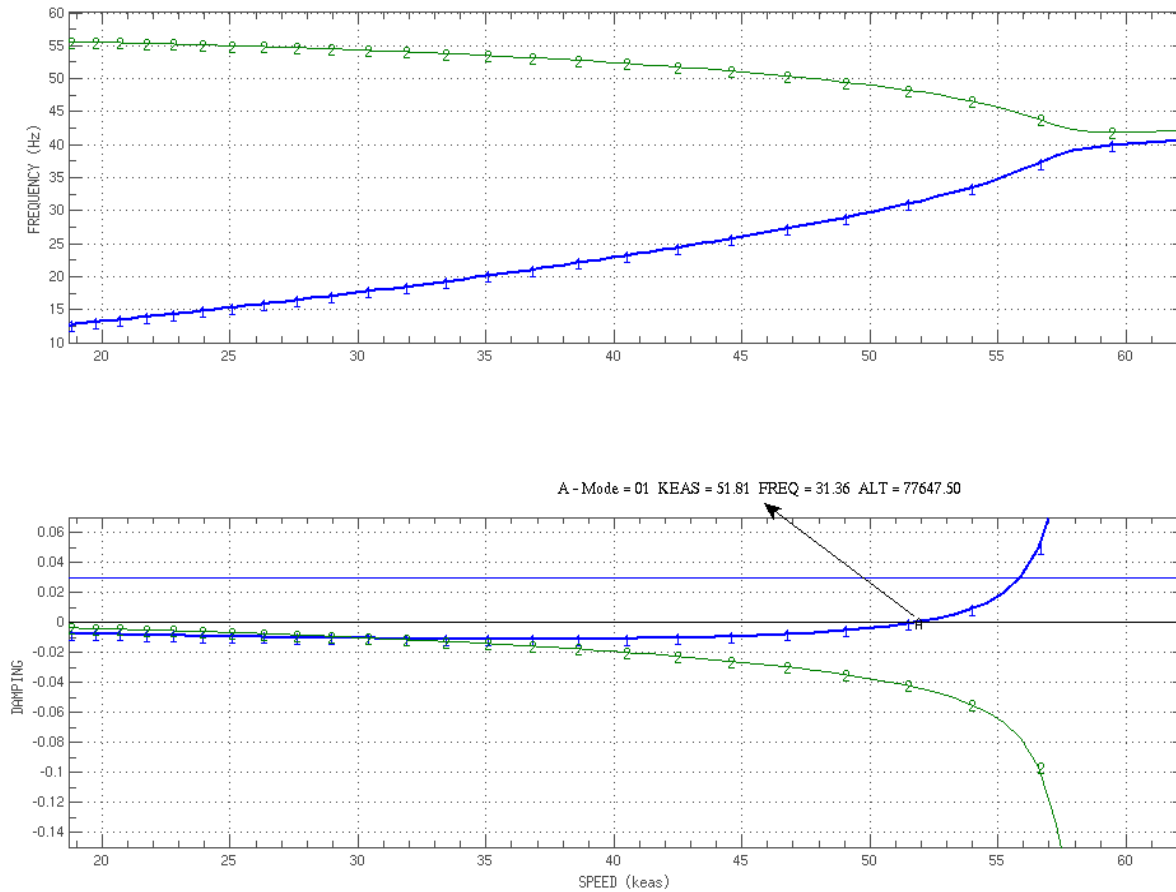


Figure 12: Closed Loop Flutter VGF plot at K = 5.06 dB showing instability at ~ 51.8 keas

4.3 Configuration # 2

The controller dynamics for this configuration is given by the following equation:

$$G_c(s) = \frac{0.01s^2 + s + 1}{s^3 + 2s^2 + s + 1} \tag{23}$$

The configuration parameters are presented in the following table:

Table 3: Cantilevered plate example – Configuration 2

Broken Loop Frequency Response	Mach 0.450 at 30.3 keas GM = 72.7 dB at 17.6 Hz
Closed Loop Flutter Analysis	Mach 0.450 - PK Method Control Law Gain Scaled by 72.7 dB Flutter Speed ~ 30.3 keas at 17.6 Hz

Figure 13 shows the broken loop frequency response plot at 30.3 keas. The plot also indicates the gain margin ~ 72.7 dB in the closed loop system. The control law is modified by scaling the scaling the control law (Equation 23) by the resulting gain margin. This gain scaled control law is then implemented in the closed flutter analysis via the PK method (Figure 14). The flutter crossing now occurs at ~30.27 keas and the numerical difference is negligible in this case.

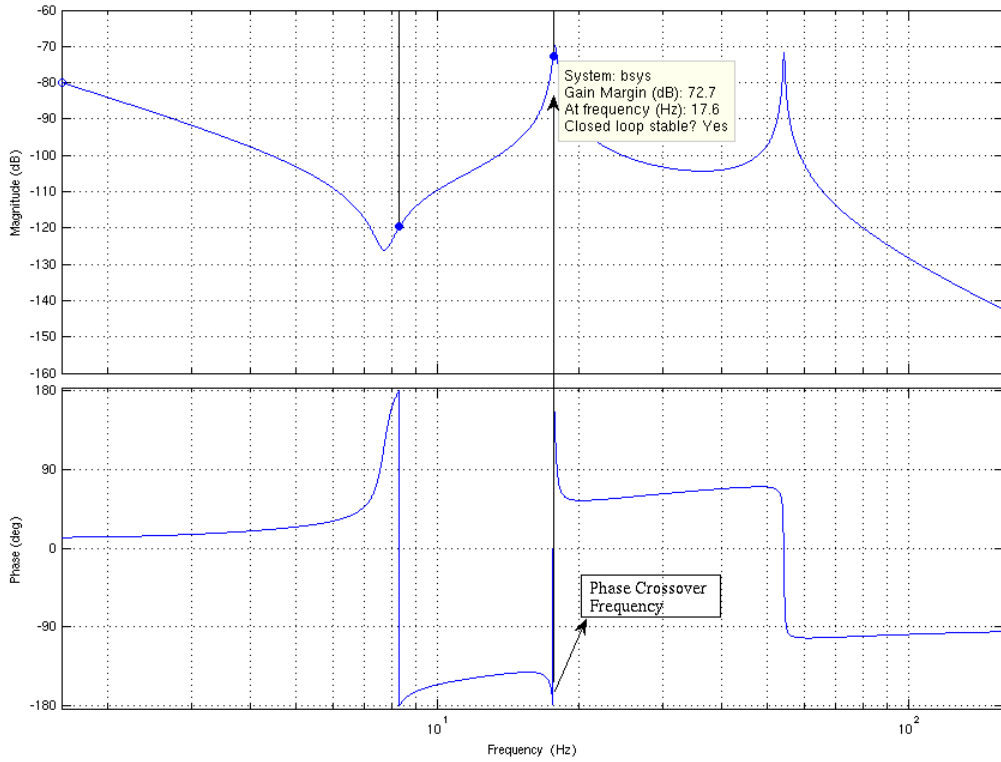


Figure 13: Broken loop stability at Mach 0.450 and 30.3 keas

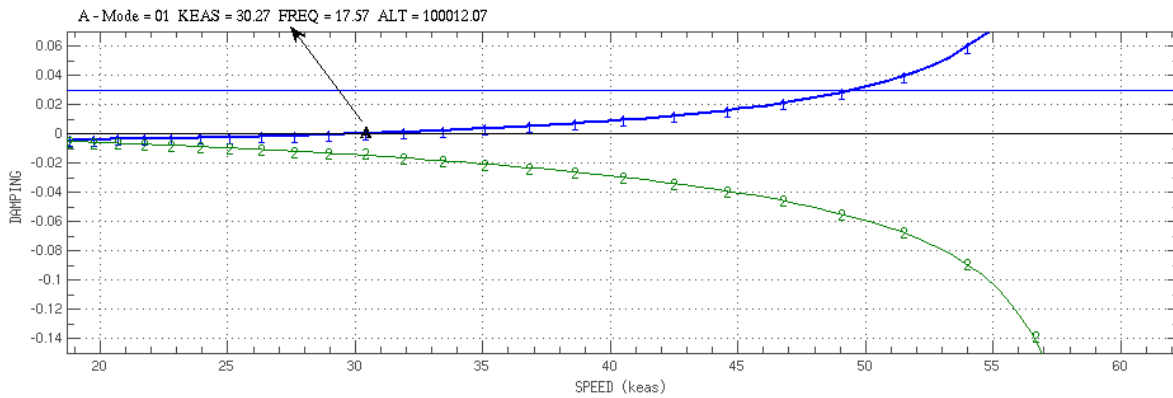
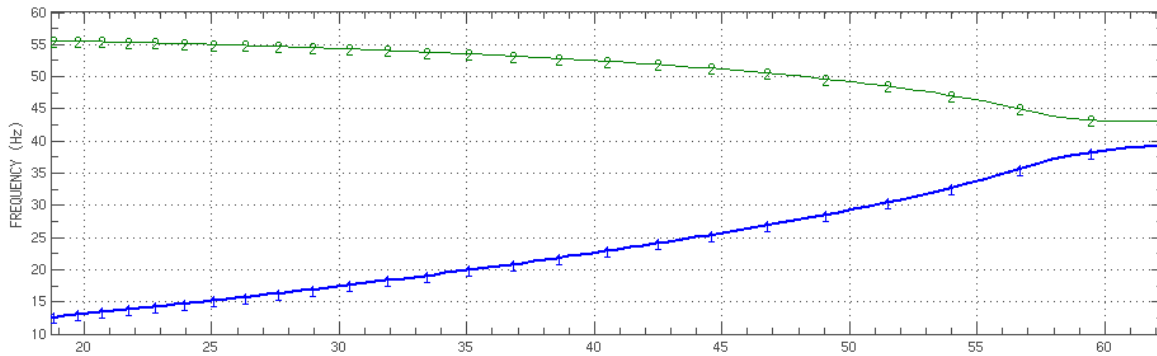


Figure 14: Closed Loop Flutter VGF plot at K = 72.7 dB showing instability at ~ 30.3 keas

4.4 Configuration # 3

The control law for this configuration is given by the following transfer function:

$$G_c(s) = \frac{0.05s^3 + 0.5s^2 + 0.005s + 0.5}{0.1s^3 + s^2 + 2s + 10} \quad (24)$$

The configuration parameters are presented in the following table:

Table 4: Cantilevered plate example – Configuration 3

Broken Loop Frequency Response	Mach 0.450 at 38.5 keas PM = -11.8° at 51.2 Hz
Closed Loop Flutter Analysis	Mach 0.450 - PK Method Pade Filter $G_{pade}(s)$ (Equation 25) for Phase Margin Control Law Multiplied by Pade Filter Flutter Speed ~ 37.8 keas (Figure 17)

Figure 15 shows the broken loop frequency response indicating a minimum phase margin of negative 11.8° at 51.2 Hz.

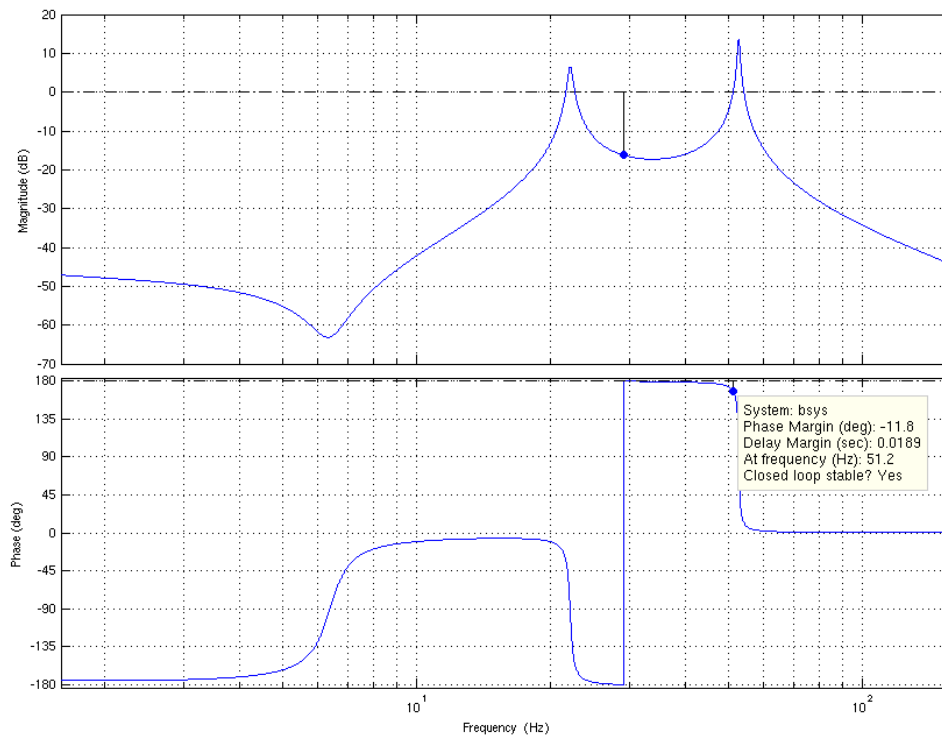


Figure 15: Broken loop stability at Mach 0.450 and 38.5 keas

The second order Pade approximation which provides the required phase shift at 51.2 Hz is given by Equation 25 and the frequency response curve corresponding to this transfer function is shown in Figure 16,

$$G_{pade}(s) = \frac{s^2 + 9400s + 2.945e7}{s^2 - 9400s + 2.945e7} \quad (25)$$

The modified control law used in the closed loop flutter analysis is the following,

$$G_{c_mod}(s) = G_{pade}(s)G_c(s) \tag{26}$$

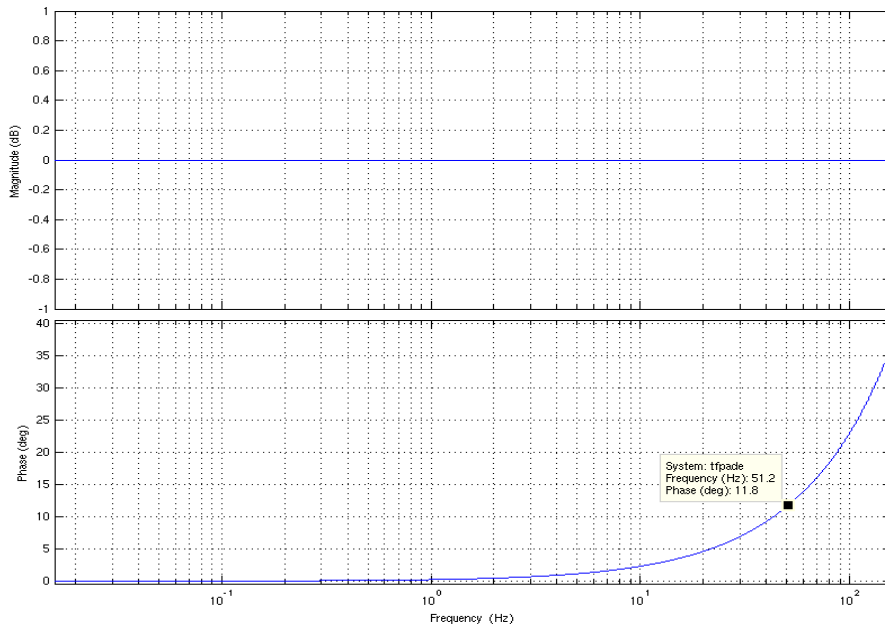


Figure 16: Pade filter frequency response indicating the required phase shift

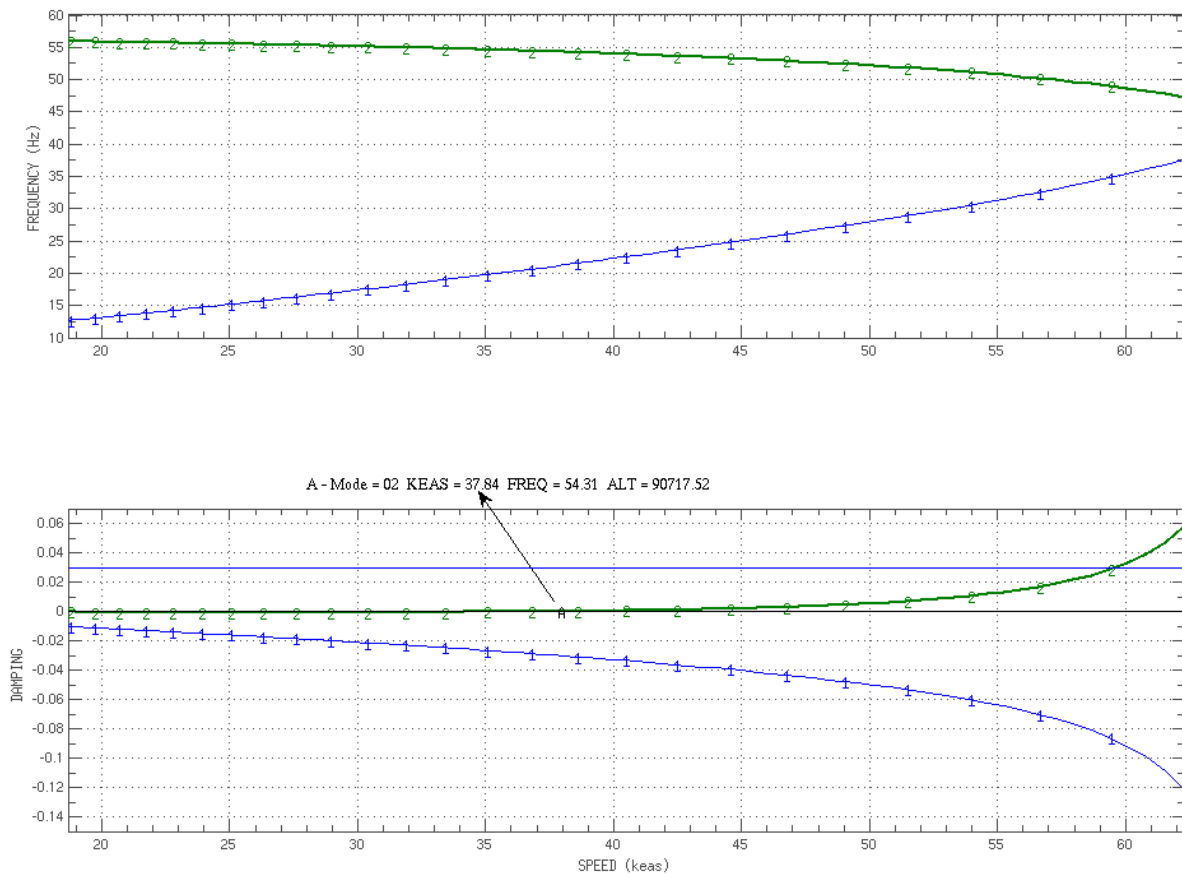


Figure 17: VGF plot for the phase shifted control law showing instability at ~ 38 keas

5 GENERIC BUSINESS JET MODEL

A more complex model both structurally and aerodynamically is considered in this section relative to the cantilevered plate model described in the previous section. The primary motive to consider this model is to demonstrate that irrespective of the model complexity, the broken loop frequency response stability analysis and the closed loop flutter analysis mathematically predict the same closed loop instability.

5.1 Model Description

This business jet example uses the aircraft symmetry about y-z plane to model only the starboard side. The wing is a composite structure and is modeled using NASTRAN's CQUAD4 elements. The fuselage is modeled as a beam (stick model) using a series of CBAR elements. The wing-fuselage interface is modeled via spring elements (CELAS). Rigid body constraints are applied along the fuselage to make the model respond only in the longitudinal direction. The mass is modeled as discrete concentrated elements along the wing, fuselage, vertical tail and horizontal tail. For the horizontal tail, only the inertial and aerodynamic effects are included and for the vertical tail only the inertial effects are included. Figure 18 shows the NASTRAN finite element model.

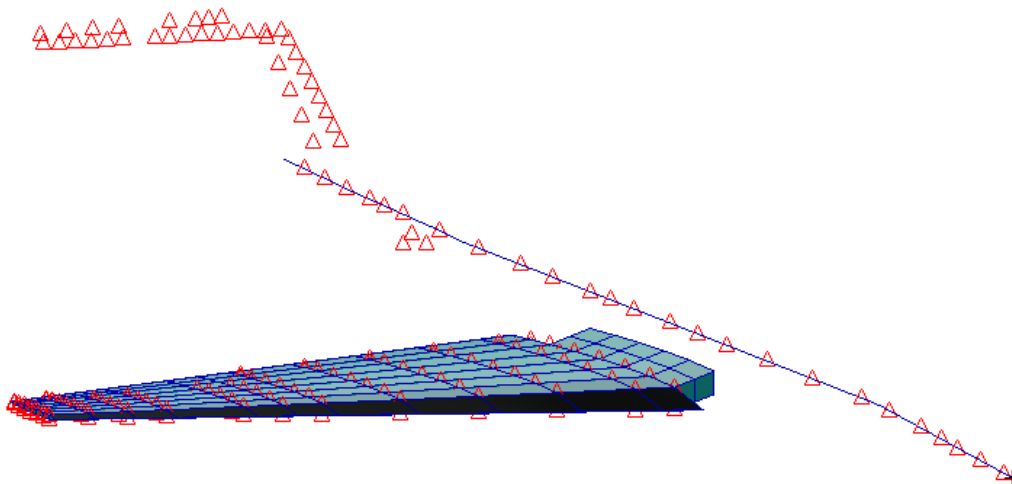


Figure 18: General Business Jet NASTRAN FEM

Similar to the previous model, the unsteady aerodynamics are modeled using the doublet lattice method. The aerodynamic model is shown in Figure 19. The control law commands only the aileron and for the aeroservoelastic analysis, only the aerodynamic coupling is included. The aileron inertial coupling is neglected. The model used in this section is a modified version of the example model documented in [15].

The open loop frequency response functions are generated with the control surface position as the input and output being the positive z-acceleration at the sensor grid located at the wing tip. For all the following configurations, the sensor definition is unchanged. To generate the open loop frequency response, state-space formulation of the aeroelastic model was utilized which was derived using Roger's method. The number of aerodynamic lag roots was set to 8. For every configuration the steps as shown in section 3.1 are executed. In addition, for this model, closed loop flutter analysis was also solved via the state space method.

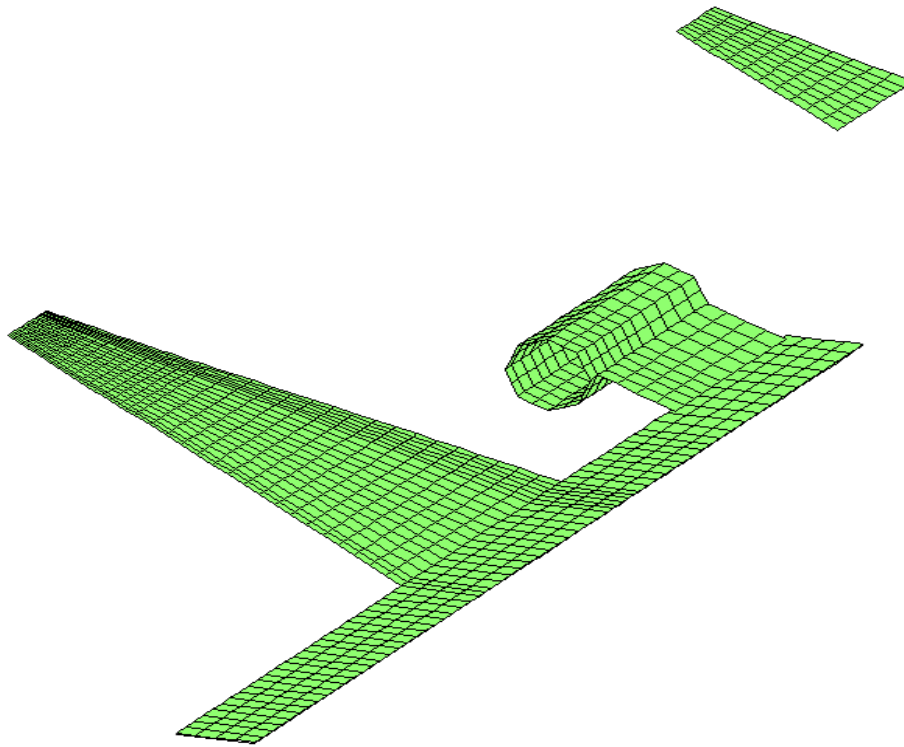


Figure 19: General Business Jet Doublet Lattice Model

5.2 Configuration # 1

The input to the control law is the wing tip acceleration (+z) and the output is the aileron deflection. The control law is given by the following transfer function:

$$G_c(s) = \frac{5.0e^{-5}s + 0.0025}{s^2 + 20s + 500} \quad (27)$$

The details of this configuration are presented in the following table:

Table 5: General Business Jet Example – Configuration 1

Broken Loop Frequency Response	Mach 0.900 at 543.06 keas (+5000 ft) GM = 75.902 at 12.98 Hz
Closed Loop Flutter Analysis	Mach 0.900 – State Space Method via Roger's Fit Mach 0.900 – Closed Loop PK method Control Law Scaled by 75.902 dB Flutter Crossing Occurs at 543.06 keas

Figure 20 shows the broken loop frequency response plot at 543.06 keas indicating a gain margin of ~ 75.9 dB in the closed loop system. The control law is modified by scaling the control law (Equation 27) by the resulting gain margin. This gain scaled control law is then implemented in the closed flutter analysis via the state space method (Figure 21) and also the PK method (Figure 22).

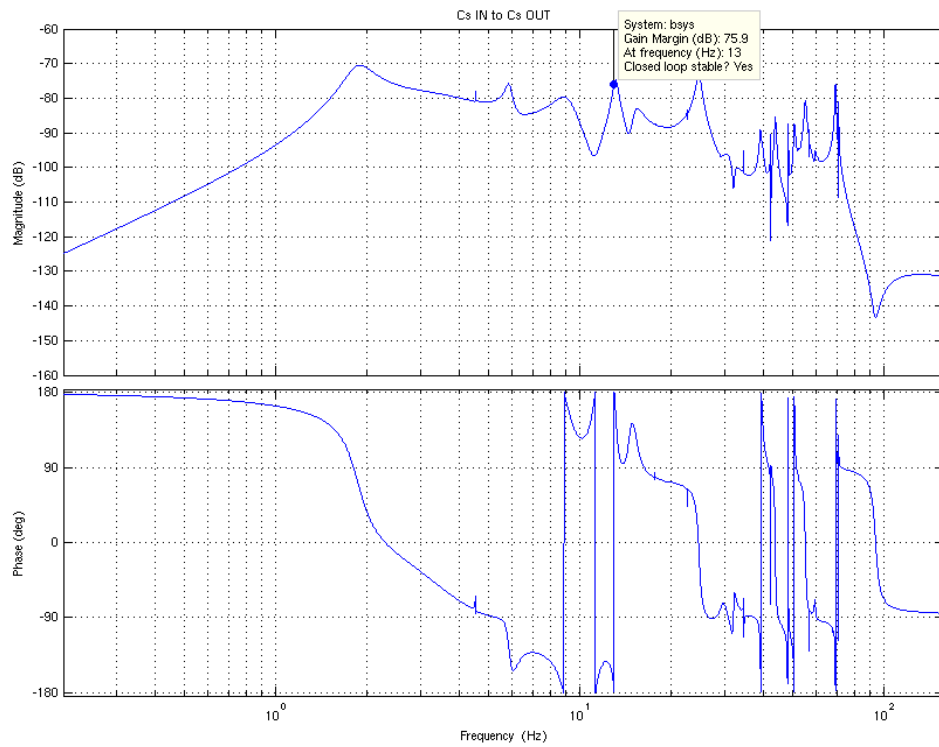


Figure 20: Broken loop frequency response stability analysis at Mach 0.9 - 543.06 keas

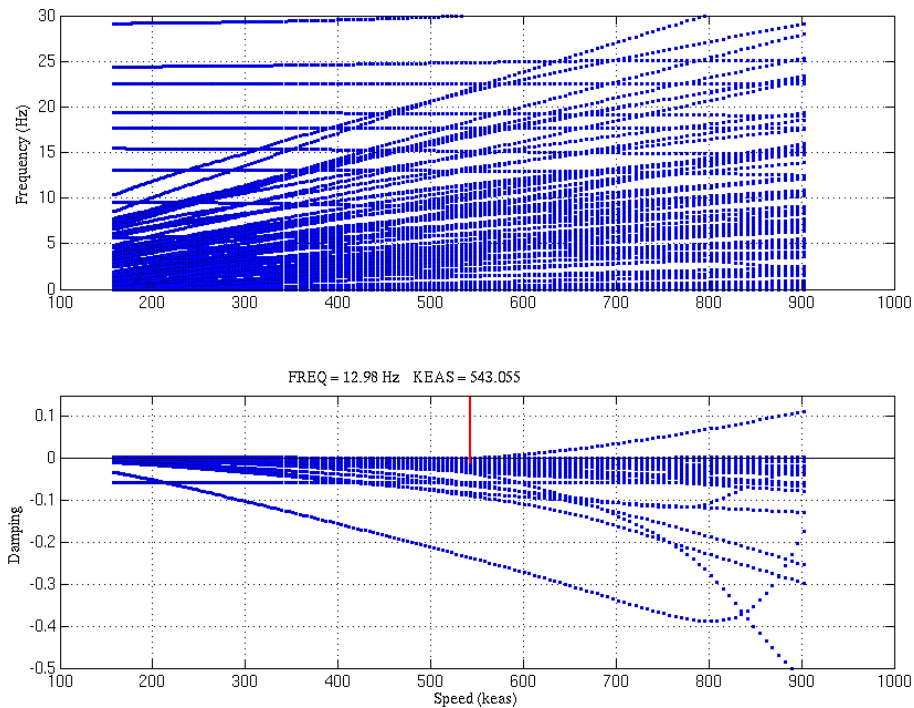


Figure 21: VGF plot via state space method -12.98 Hz at 543.06 keas

The flutter crossing occurs at exactly the same speed 543.06 keas in the case of the state space method due to the fact that both methods (the broken loop frequency response generation) use the same rational function approximation (Roger’s fit) for the unsteady aerodynamics. For the PK method, the difference in the flutter speed is less than 1% compared to the state space approach. This numerical difference is due to iterative nature of the PK method and the fact

that the aerodynamic forces are fit using rational function approximation for the plant FRF. VGF plots resulting from the state space method and the closed loop PK method are shown in Figure 21 and Figure 22 respectively.

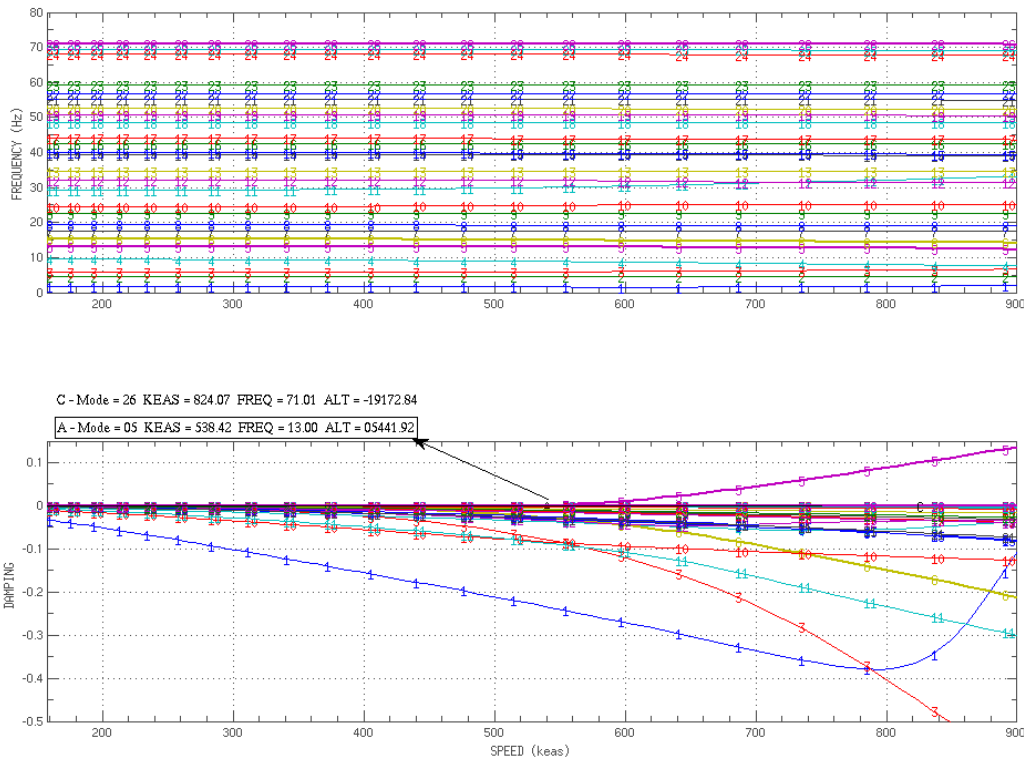


Figure 22: VGF plot via PK method – 13.00 Hz at 538.4 keas

5.3 Configuration # 2

Except the control law, all the parameters including the sensor definition are exactly the same as the previous configuration. The control law is given by the following transfer function:

$$G_c(s) = \frac{0.01s^2 + 0.065s + 0.01}{s^3 + 10s^2 + 50s + 100} \quad (28)$$

The details of this configuration are presented in the following table:

Table 6: General Business Jet Example – Configuration 2

Broken Loop Frequency Response	Mach 0.900 at 673.62 keas (-7000 ft) GM = 25.9 at 13.20 Hz
Closed Loop Flutter Analysis	Mach 0.900 – State Space Method via Roger’s Fit Mach 0.900 – Closed Loop PK method Control Law Scaled by 25.9 dB Flutter Crossing at 673.61 keas (State Space Method) Flutter Crossing at 678.73 keas (PK Method)

Figure 23 shows the broken loop frequency response plot at 673.62 keas indicating a minimum gain margin of ~ 25.9 dB at 13.2 Hz. The control law is modified by scaling the scaling the control law (Equation 28) by the resulting gain margin. This gain scaled control

law is then implemented in the closed flutter analysis via the state space method (Figure 24) and also the PK method (Figure 25).

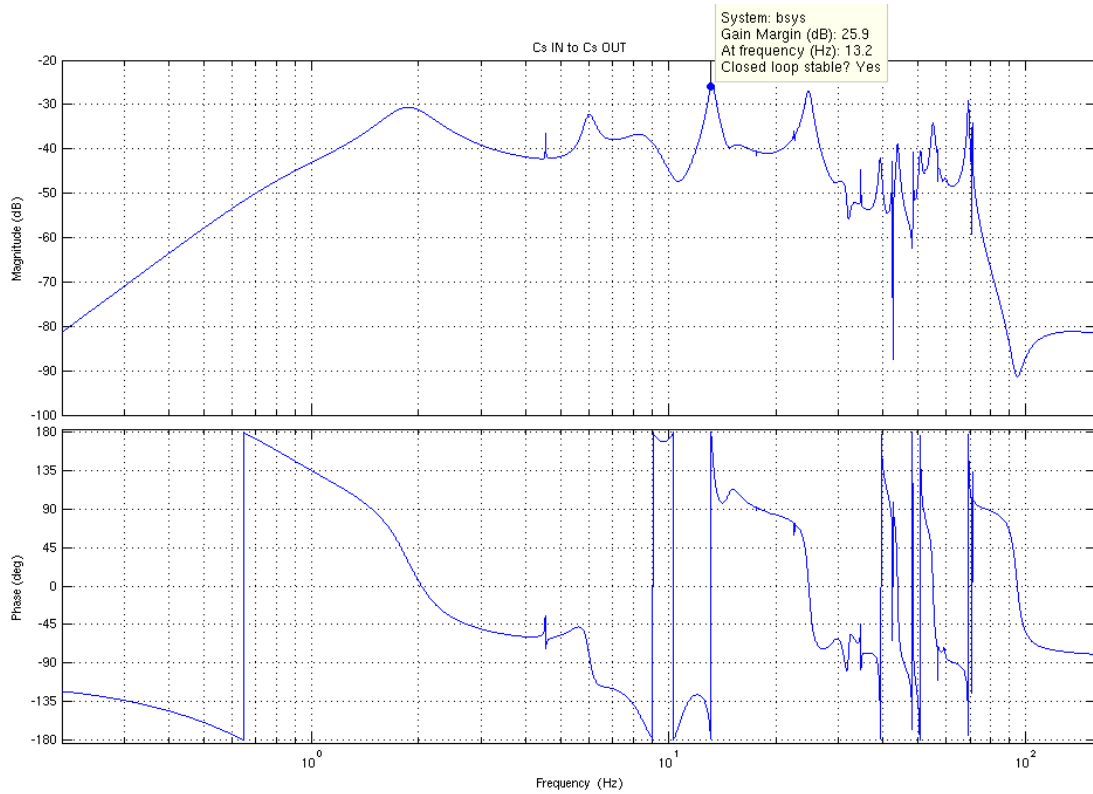


Figure 23: Broken loop frequency response stability analysis at Mach 0.9 – 673.61 keas

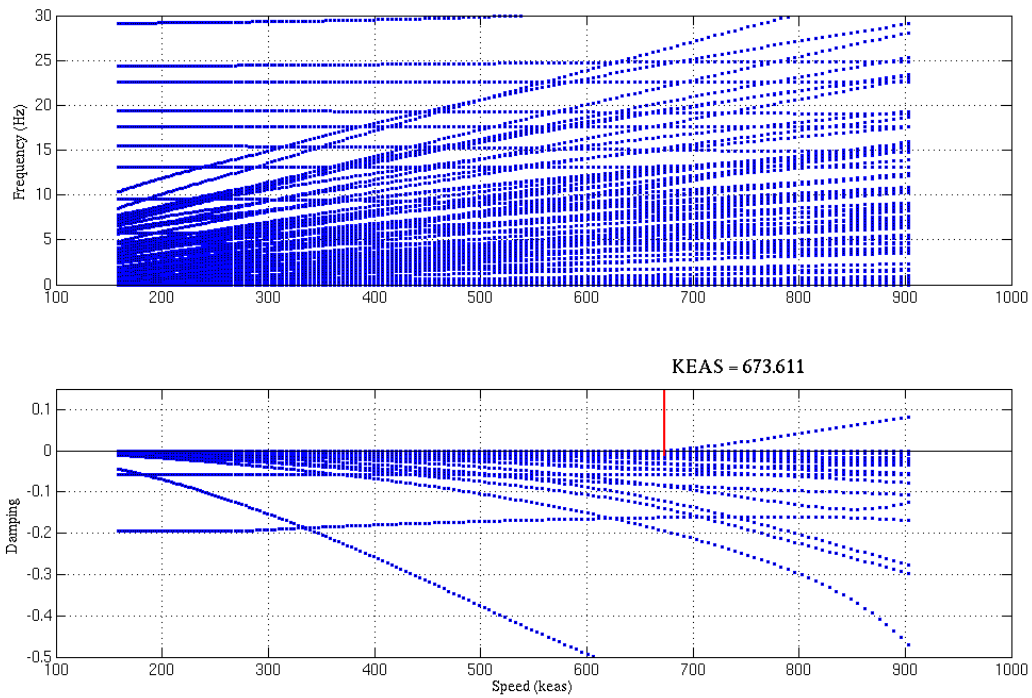


Figure 24: VGF plot via state space method –13.2 Hz at 673.61 keas

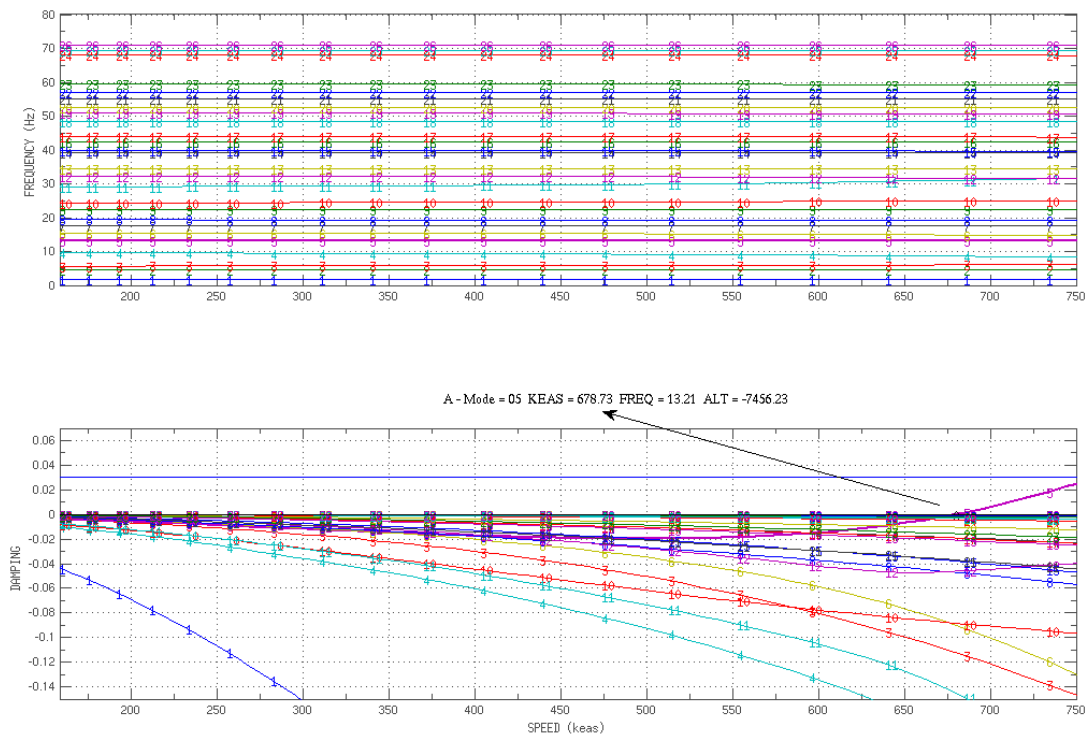


Figure 25: VGF plot via PK method – 13.21 Hz at 678.73 keas

The flutter crossing occurs at 673.61 keas in the case of the state space method. For the PK method, the difference in the flutter speed is less than 1% compared to the state space approach, similar to what was presented in the previous sections.

6 SUMMARY

Two methods of assessing the aeroservoelastic stability problem are presented in this paper 1) Closed loop flutter analysis and 2) Broken loop frequency response stability analysis. The gain and phase margins predicted by the broken loop approach can be inferred as the measure of the robustness of the aeroservoelastic system. Three aeroelastic example systems have been considered with increasing complexity, starting from a two degree of freedom system to a large aircraft model. Irrespective of model complexity, the two methods have shown that the dynamic pressure at which the aeroservoelastic instability occurs did not differ between the methods.

Both methods can be easily applied to Single-Input-Single-Output (SISO) systems and in fact the terms gain and phase margin were originally intended to be applicable to SISO systems. With advances in the control law design, MIMO systems are inevitable and applying the broken loop approach to MIMO systems requires determination of “where to break the loop”. Various approaches exist on how to deal with breaking MIMO control law loops, for example, opening one specific loop while other loops closed or opening all the loops at the same time. Nonetheless, the broken loop frequency response stability analysis can be applied to the MIMO systems.

Efficiency and flexibility are the two primary advantages of the broken loop frequency approach over the closed loop flutter analysis. “Efficiency” comes from the fact that the broken loop analysis utilizes the aeroelastic frequency response functions in which the dynamics of the complex aeroelastic system are captured and simply multiplied by the specific loop of the control law frequency response. Further, a number of established control

centric techniques exist, such as root locus, Bode or Nyquist, to assess the stability of the closed loop system. Closed loop flutter algorithms typically require adding a large number of control law degrees of freedom to the already existing flexible modes thereby demanding extensive eigenvalue sorting and tracking. “Flexibility” comes from the fact that the broken loop analysis approach can easily integrate various control law configurations or loops and allows for rapid assessment of the closed loop stability. In addition, the broken loop approach reveals the stability margin of all of the aeroelastic modes at a given flight condition, something that closed loop flutter analysis does not provide.

One of the major drawbacks of the closed loop flutter analysis is the amount of computational runs required to analyze various gain and phase variations introduced into the control law to establish closed loop stability. Even if a discrete set of gains, for example, $K_1 < K_2 < K_j \dots < K_N$ are introduced into the control law and the flutter analysis does not show any crossing or instability, this does not guarantee the stability for all the gains K_i where $K_j < K_i < K_{j+1}$. This misinterpretation could possibly lead to unstable aeroservoelastic system when analyzing the system for robustness through closed loop flutter analysis.

In comparison to the broken loop approach, one advantage of the closed loop flutter analysis is that it can present the effect of the control law on the flutter mode frequency and damping similar to an open loop VGF curve due to the fact that the method tracks eigenvalue of the closed loop system as a function of dynamic pressure.

7 REFERENCES

- [1] Tewari, A. (2015). *Aeroservoelasticity: Modeling and Control*. New York: Springer-Verlag.
- [2] Mukhopadhyay, V., Livine, E. (2010). *Aeroservoelasticity, Encyclopedia of Aerospace Engineering*. Wiley & Sons.
- [3] Livine, E. (2017). Aircraft active flutter suppression state of the art and technology maturation Needs. 58th AIAA/ASCE/AHS/ASC Structures, Structural Dynamics and Materials Conference.
- [4] Dale, M., P., William, B., H., Charles, E., G. (2003). F/A-18/E/F Aeroservoelastic Design, Analysis and Test. 44th AIAA/ASCE/AHS/ASC Structures, Structural Dynamics and Materials Conference, The Boeing Company.
- [5] Astrom, K., J., Murray, M., R. (2008). *Feedback Systems: An Introduction for Scientists and Engineers*. Princeton University Press.
- [6] Rodden, P., W. (2011). *Theoretical and Computational Aeroelasticity*. Crest Pub.
- [7] Rodden, P., W., Erwin, H., J. (2009) *Aeroelastic Analysis User's Guide*. MSC NASTRAN.
- [8] Tiffany, S., Adams, W. (1988). Nonlinear programming extensions to rational function approximation of unsteady aerodynamics. TP-2776, NASA.
- [9] Cotoi, I., Botez, R. (2002). Method of unsteady aerodynamic forces approximation for aeroservoelastic interactions. *AIAA Journal of Guidance, Control and Dynamics*, 25(5), 985-987.
- [10] Roger, K., L. (1977). Airplane math modeling methods for active control design. AGARD CP-228, Structural Aspects of Active Control. 4-1-4-11

- [11] Vepa, R. (1977). Finite state modeling of aeroelastic system. CR-2779, NASA.
- [12] Karpel, M. (1982). Design for active flutter suppression and gust alleviation using state-space aeroelastic modeling. *Journal of Aircraft*, 19(3), 221–227.
- [13] Hancock, G. J., Wright, J. R., Simpson, A. (1985). On the teaching principles of wing flexure-torsion flutter. *Aeronautical Journal*, October 1985, 285–305.
- [14] Wright, J. R., Cooper, J. E. (2007). *Introduction to Aircraft Aeroelasticity and Loads*. Wiley.
- [15] Zona Technology Inc. (2018). *ZAERO Application's Manual Vol.2*.

COPYRIGHT STATEMENT

The authors confirm that they, and/or their company or organization, hold copyright on all of the original material included in this paper. The authors also confirm that they have obtained permission, from the copyright holder of any third party material included in this paper, to publish it as part of their paper. The authors confirm that they give permission, or have obtained permission from the copyright holder of this paper, for the publication and distribution of this paper as part of the IFASD-2019 proceedings or as individual off-prints from the proceedings.